Braz J Phys (2012) 42:110–119
DOI 10.1007/s13538-012-0062-5

SBF SOCIEDADE BRASILEIRA DE FÍSICA

PARTICLES AND FIELDS

Loop Expansion in Yang–Mills Thermodynamics

Ralf Hofmann

Received: 27 September 2011 / Published online: 26 January 2012

Abstract We argue that a self-consistent spatial coarse graining, which involves interacting (anti)calorons of unit topological charge modulus, implies that real-time loop expansions of thermodynamical quantities in the deconfining phase of SU(2) and SU(3) Yang–Mills thermodynamics are, modulo one-particle irreducible resummations, determined by a finite number of connected bubble diagrams.

Keywords Thermal ground state · Adjoint Higgs mechanism · Algebraic geometry · Mandelstam variables · UV finiteness · IR finiteness

1 Introduction and Mini-Review

A reliable approximation of the high-temperature thermodynamics related to four-dimensional pure Yang–Mills theories in terms of a small-coupling expansion is impossible[1] [1]. The nonconvergence of the small-coupling expansion is tied to the fact that a too naive *a priori* estimate—an empty (trivial) ground state—is invoked to construct an approximating series for the full partition function. Recall that fluctuations of nontrivial topology, having a profound impact on the ground-state estimate, are completely ignored in small-coupling expansions because their weight possesses an essential zero at vanishing coupling. As a consequence, the strongly correlating effects of these extended field configurations [2] are completely ignored: A fact which is expressed by the tree-level masslessness and only weak radiative screenings of all gauge bosons leading to the nonconvergence of the expansion. Loosely speaking, the physical expansion parameter, which is not the small coupling constant but the ratio of the typical action of a quantum fluctuation to $\hbar$, is not guaranteed to be small due to the unconstrained dynamics of massless gauge bosons.

The purpose of the present work is to provide arguments on why an *a priori* estimate for the ground state of an SU(2) Yang–Mills theory at high temperatures (deconfining phase[2]), which is obtained by a self-consistent and sufficiently local spatial coarse graining[3] over interacting and stable Bogomol'nyi–Prasad–Sommerfield (BPS)-saturated topological field

R. Hofmann (✉)
Institut für Theoretische Physik, Universität Heidelberg, Philosophenweg 16, 69120 Heidelberg, Germany
e-mail: r.hofmann@thphys.uni-heidelberg.de

[1] We restrict our discussion to the gauge group SU(2). Larger groups can, in principle, be investigated by the identification of possible SU(2) embeddings. In fact, our results of Sections 2 and 3 are also valid for SU(3), compare with [4, 5]. However, for SU(N), N ≥ 4, the phase diagram is not unique, and hence, the concept of just one deconfining phase is false [4, 5].

[2] We refrain here from discussing in detail the other two phases, preconfining and deconfining; see [4, 5]. While thermodynamical quantities are one-loop exact in the preconfining phase, there exist asymptotic expansions in the confining phase; see, for example, [3].

[3] This refers to the fact that only configurations with topological charge modulus $|Q| = 0, 1$ need to be taken into account; see below.

configurations, leads to a rapidly converging loop expansion. This claim rests on the self-consistent emergence of a temperature-dependent scale of maximal resolution which also generates a mass gap on tree-level (adjoint Higgs mechanism) for the two off-Cartan modes in unitary gauge (ultraviolet and infrared cutoff). Both effects imply that the typical action of residual quantum fluctuations in the effective theory is small.

Before we start the present discussion, we consider it helpful to remind the reader of the dynamical situation leading to the emergence of a highly nonperturbative ground state even at large temperatures, $T \gg \Lambda$. Here Λ denotes the Yang–Mills scale [4–6]. Stable, that is, BPS-saturated topological defects of a trivial holonomy (or Harrington–Shepard (HS) (anti)calorons with $|Q| = 1$) [7] interact by large-scale (compared to the scale parameter ρ) gluon exchanges. This generates dynamical magnetic substructure in the (anti)calorons whose motion [8] is determined by short-scale gluon fluctuations.[4] At the same time, the presence of (anti)calorons induces consecutive scatterings of all those gluons that are sufficiently close to their mass shell to propagate over large distances. Upon a self-consistent spatial coarse graining, the former situation identifies ground-state pressure and the ground-state energy density with those of a linearly dependent-on-temperature cosmological constant. The ground state's effect on long-distance gauge-mode propagation is the generation of mass in the off-Cartan directions (adjoint Higgs mechanism in unitary gauge).

Both phenomena, the generation of a finite energy density of the ground state and the emergence of mass, are described by the BPS-saturated, classical dynamics of a spatially homogeneous and adjoint scalar field ϕ and a pure-gauge configuration[5] a_μ^{bg}. The reader may wonder why the macroscopic field ϕ is in the adjoint representation of the gauge group (after coarse graining, the gauge rotations of ϕ are only dependent on Euclidean time τ [4–6]). The answer to this question is rooted in the perturbative renormalizability of the Yang–Mills theory to any loop order [9–11], which guarantees that, after coarse graining, propagating gauge fields of trivial topology are in the same representation as the gauge fields defining the fundamental action: Fundamental and coarse-grained gauge modes simply differ by a wave-function renormalization. A gauge-invariant coupling to the inert, coarse-grained sector with $|Q| = 1$ thus is only possible by a covariant derivative for either a fundamental or an adjoint scalar. Since ϕ is a (nonlocal!) composite of the fundamental field strength, the former possibility is ruled out (no spin-1/2 part in products of spin-1 representations).

Technically, the coarse graining over noninteracting[6] HS (anti)calorons is performed in two steps: (a) Determine the differential operator $\mathcal{D}$ whose kernel $\mathcal{K}$ contains ϕ's phase $\hat{\phi}$ in terms of a unique definition of $\mathcal{K}$ involving a ρ and an infinite space average over

[4] Nontrivial holonomy is associated with a mass scale $\propto T$ expressing itself in singular gauge by the Polyakov loop at spatial infinity not coinciding with a member of the SU(2) center $-$, . The A_4-component of the (anti)caloron configuration then effectively serves as an adjoint Higgs field. As a consequence, a BPS monopole and its antimonopole emerge which are spatially separated if ρ does not vanish [12–17]. By computing the one-loop quantum weight for a nontrivial-holonomy SU(2) caloron, it was shown in [18] that a small (anti)caloron holonomy induces attraction between the monopole and its antimonopole while a large holonomy yields repulsion. While the likelihood of the former situation is determined by the quantum weight of a HS caloron and thus, depending on ρ and T, can be of order unity [19], the probability for repulsion is estimated by a Boltzmann factor $\sim e^{-40}$ [4, 5]: The by-far dominating situation is monopole–antimonopole attraction which drives the (anti)caloron back to trivial holonomy (monopole–antimonopole annihilation). The rare process of (anti)caloron dissociation by monopole–antimonopole repulsion generates isolated (anti)monopoles whose magnetic charge is screened by intermediate small-holonomy (anti)calorons. Despite the fact that there is an extremely small ratio of the number of stable and the number of to-be-annihilated monopoles at any instant of time and at any temperature ($T \gg \Lambda$), the absolute density of stable and screened monopoles increases with temperature [4, 5]. This may lead to the lattice-observed phenomenon of a spatial string tension rising as T^2 [20]; see [21, 22] for the deep theoretical reasons. An accordingly microscopic model was constructed in [23]. This model builds on the existence of a typical spatial volume inhabited by a dissociated, large-holonomy (anti)caloron with $|Q| = 1$ [4, 5].

[5] Quantum and statistical fluctuations of the field ϕ are proven to be absent at the resolution $|\phi|$ [4, 5].

[6] To assume a starting situation for the coarse-graining process, where (anti)calorons are noninteracting, turns out to be self-consistent: The emerging, macroscopic field ϕ is inert, that is, not deformable by the microscopic interactions between (anti)calorons [4, 5].

HS (anti)calorons[7] entering in the definition of an adjoint two-point function of the field strength [4–6] and (b) assume the existence of a Yang–Mills scale Λ to self-consistently determine $|\phi|(T,\Lambda)$ by identifying the kernel $\mathcal{K}'$ of a "square root" of $\mathcal{D}$ (BPS saturation, still noninteracting HS caloron and anticaloron). The resolution $|\phi|$ is optimal in the sense that it sets a length scale $|\phi|^{-1}$ at which the infinite spatial coarse graining, used to define the phase $\hat{\phi}$, is saturated and at the same time assures that the coarse graining is sufficiently local such that fundamental (anti)selfdual configurations with $|Q|>1$ need not be taken into account. Namely, expressing the spatial ultraviolet cutoff $|\phi|^{-1}=\sqrt{\frac{2\pi}{\Lambda^3\beta}}$ in units of $\beta\equiv 1/T$ yields 8.22 at the critical temperature T_c; for $T>T_c$, this number grows as $(T/T_c)^{3/2}$. But for integration cutoffs $\rho_u\sim r_u\geq 8.22\,\beta$, the kernel $\mathcal{K}$ practically coincides with that of the infinite-volume limit; see [4–6]. Here r_u denotes the infrared cutoff in the radial part of the space integral defining $\hat{\phi}$. Finally, one shows the above-mentioned fluctuation inertness of the field ϕ by means of its effective action whose potential is uniquely fixed.[8]

Two parameters, the *effective* coupling e and the Yang–Mills scale Λ (through the potential $V(\phi)$), enter the effective action. While the latter is a free parameter of the theory,[9] the former is subject to an evolution in temperature. To derive the associated evolution equation, we need to discuss the effects on the (quasiparticle) spectrum of the above a priori estimate for the ground state.

First, one observes that a singular but admissible gauge transformation de-winds the field ϕ to lie in fixed direction on the group manifold (no τ dependence). At the same time, a_μ^{bg} is gauged to zero (unitary gauge). As an aside, one proves the deconfining nature of the discussed phase of the theory: The ground-state expectation of the Polyakov loop is, indeed, Z_2 degenerate. In unitary gauge, the physical spectrum of excitations is identified: For SU(2), two out of three-color directions acquire masses by the adjoint Higgs mechanism. We will refer to the massless direction as tree-level massless (TLM) and to the massive one as tree-level heavy (TLH) (thermal quasiparticles). A completely physical gauge is reached by prescribing the Coulomb condition for the unbroken $\mathrm{U}(1)\subset\mathrm{SU}(2)$. Thermodynamical quantities now are loop-expanded in terms of residual $Q=0$ fluctuations. That is, the process of integrating out these fluctuations is organized as a formal expansion in powers of $\hbar^{-1}$ and not in e. In unitary-Coulomb gauge, there are conditions for the maximal off-shellness of fluctuations and for the maximal momentum transfer in four vertices; see Section 2. Second, the invariance of Legendre transformations between thermodynamical quantities under the applied spatial coarse graining is assured by the stationarity of the pressure with respect to variations in the Higgs mechanism-induced quasiparticle masses. This condition generates an equation for the evolution of e with temperature. As a consequence, a decoupling of ultraviolet from infrared physics occurs. That is, e's evolution at lower temperatures is independent of the physics taking place at a specifically chosen high temperature [4, 5].

The paper is organized as follows: In the next section, we discuss and set up the constraints on the loop momenta for coarse-grained trivial-topology fluctuations as they emerge in the effective theory in unitary-Coulomb gauge. In Section 3, we argue that the resummation of one-particle irreducible (1PI) contributions to the polarization tensor generates broadened spectral functions for each propagating mode and thus

[7] The dimensionless quantity $\hat{\phi}$ depends on temperature only via the periodicity in τ. This implies that dimensional transmutation does not play a role in the emergence of $\hat{\phi}$. Thus, $\hat{\phi}$ is obtained from an average over absolutely stable, classical field configurations: HS calorons. The definition of $\hat{\phi}$ (see [4–6]) excludes the contribution of BPS-saturated configurations with $|Q|>1$. This is consistent with the final result that the field ϕ emerges due to a sufficiently local coarse graining down to a resolution $|\phi|$ such that multiple bumps of topological charge density do not enter the process. The integration over shifts of the (anti)caloron center is dimensionally forbidden. A fixed shift of the center w.r.t. the spatial origin can be related to the unshifted situation by an appropriate parallel transport which does not alter $\mathcal{D}$. The computation requires the introduction of various regularizations. A regularization of the azimuthal angular integration seems, at first sight, to break rotational invariance by the introduction of an axis. However, one can show that a rotation of this axis within the azimuthal plane is just a global gauge transformation of ϕ's phase. Thus, any rotated axis would have yielded the same physics. As a consequence, no breaking of rotational symmetry is introduced by the regularization of the azimuthal angular integration.

[8] No freedom of shifting the ground-state energy density exists because of the BPS saturation of the field ϕ, and the inertness of ϕ already is a consequence of the nonpropagating nature of (anti)calorons: their energy-momentum tensor vanishes identically.

[9] Possibly derivable from the Planck mass M_P if the emergence of gravity and matter will ever be understood in terms of a dynamical breaking of an infinite gauge symmetry.

evades the problem of pinch singularities (powers of delta functions). In Section 4, we generate a lower and an upper estimate for the ratio of the number of independent radial loop-momenta components to the number of constraints as a function of the number of vertices in bubble diagrams with resummed one-particle irreducible insertions. These estimates strongly suggest that only a finite number of such diagrams contribute to the loop expansion. An investigation of two example diagrams is performed in Section 5, one with a noncompact support for the radial loop momenta integration and one where this integration is supported by a compact region. In Section 6, we briefly summarize our results and give our conclusions.

2 Constraints on Loop Momenta

Here we discuss how and which constraints emerge for the propagation and interaction of coarse-grained, topologically trivial fluctuations in the effective theory. It is essential to note that the implementation of momentum constraints on residual fluctuations, arising due to a limited resolution, can only be performed if a real-time treatment of these fluctuations is applied. Only then is it possible to discern quantum from thermal fluctuations.

The concept of a resolving power R attached to a probe is based on the uncertainty relation:

$$\Delta x \Delta p \sim 1 \quad \Leftrightarrow \quad \Delta p \sim \frac{1}{x} \equiv R\,. \tag{1}$$

Here Δp refers to the average *deviation* of the probe momentum from the situation where the probe would move along a classical trajectory subject to a certain momentum distribution. In the case of a free theory, Δp is the deviation from the mass shell:

$$\Delta p = \sqrt{|p^2 - m^2|}\,. \tag{2}$$

Two sorts of observations are important: (a) In the effective theory, which is obtained by averaging over fluctuations with resolving power Δp larger than the scale $|\phi|$, we need to consider only those modes with $\Delta p \leq |\phi|$ for otherwise we would double-count propagating fluctuations. (b) Since the process of coarse graining generates particle masses only for $\Delta p \leq |\phi|$, we need to make sure that an intermediate *massless* particle in the fundamental theory, which as a massive particle does not exist in the effective theory and thus dresses a vertex such that the latter appears to be *local*, does not possess a resolving power larger than $|\phi|$ in the fundamental theory for otherwise the vertex would no longer appear to be local.[10] Notice that the requirement $|p^2| \leq |\phi|^2$ for the massless mode in the fundamental theory indeed implies that in the effective theory, the massive mode with the same momentum is far away from its mass-shell and thus does not exist.

To work observations (a) and (b) into quantitative constraints a completely fixed, a physical gauge must be used. The absorption of the would-be Goldstone mode into the longitudinal component of the gauge field, emerging due to the apparent dynamical gauge symmetry breaking SU(2)→U(1), is facilitated by an admissible rotation to unitary gauge $\phi \equiv \lambda_3 |\phi|$, $a_\mu^{g.s.} = 0$ [4, 5]. In this gauge, the spectral manifestation of the symmetry breaking is a quasiparticle mass for two out of three directions in the algebra. The remaining U(1) gauge freedom for fluctuations δa_μ^3 is fixed by the Coulomb condition $\partial_i \delta a_i^3 = 0$.

Quantitatively, observation (a) then is expressed as

$$\begin{aligned} \left|p^2 - m^2\right| &\leq |\phi|^2 \quad \text{(for a TLH mode)}\,, \\ \left|p^2\right| &\leq |\phi|^2 \quad \text{(for a TLM mode)} \end{aligned} \tag{3}$$

where $|\phi| = \sqrt{\frac{\Lambda^3}{2\pi T}}$. For three vertices, (b) is already contained in (a) by momentum conservation in the vertex. For four vertices, the implementation of observation (b) is more involved because one needs to distinguish s, t, and u channels in the scattering process. Suppose that the ingoing (outgoing) momenta are labeled by p_1 and p_2 (p_3 and $p_4 = p_1 + p_2 - p_3$). Then the following three conditions emerge

$$\begin{aligned} \left|(p_1 + p_2)^2\right| &\leq |\phi|^2 \quad (s \text{ channel}) \\ \left|(p_3 - p_1)^2\right| &\leq |\phi|^2 \quad (t \text{ channel}) \\ \left|(p_2 - p_3)^2\right| &\leq |\phi|^2 \quad (u \text{ channel})\,. \end{aligned} \tag{4}$$

Notice that the three conditions in (4) reduce to the first condition if one computes the one-loop tadpole contribution to the polarization tensor or the two-loop contribution to a thermodynamical quantity, say the pressure, arising from four vertices [24–26]. Namely, the t-channel condition is then trivially satisfied while the u-channel condition reduces to the s-channel con-

[10] At $T = 0$ and in pure perturbation theory, this goes under the name renormalization at the scale μ where μ is determined by the maximal resolving power associated with the process under investigation. In the deconfining phase of Yang–Mills thermodynamics, the resolving power $|\phi|$ self-consistently emerges as a function of T and Λ; see below and [4, 5].

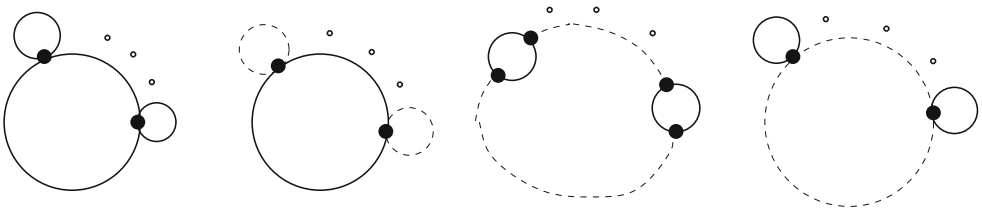

Fig. 1 Ring-diagrams as they occur in a loop expansion of the pressure in SU(2) Yang–Mills thermodynamics. *Solid* (*dashed*) *lines* are associated with TLH- (TLM-) mode propagation

dition by letting the loop momentum $k \to -k$ in $|(p-k)^2| \leq |\phi|^2$; see [4, 5, 24–26].

Notice that upon a Euclidean rotation $p_0 \to ip_0$, the first condition in (3) goes over in

$$\left|p^2 + m^2\right| \leq |\phi|^2. \tag{5}$$

For SU(2), the quasiparticle mass is given as $m = 2e\,|\phi|$ with $e \geq 8.89$ [4, 5]. Thus, condition (5) is never satisfied, and TLH modes propagate on-shell only.[11]

3 Pinch Singularities

Here we would like to point out that the occurrence of powers of delta functions of the same argument, as they appear when real-time expanding the pressure into loops, can be resolved by appropriate resummations.

The problem occurs in the so-called ring diagrams; see Fig. 1.

At tree levels, the propagators of a TLH or a TLM mode are given as [25, 26]:

$$D^{\mathrm{TLH},0}_{\mu\nu,ab}(p) = -\delta_{ab}\,\tilde{D}_{\mu\nu}\left[\frac{i}{p^2-m^2} + 2\pi\delta\left(p^2-m^2\right) n_B\left(|p_0|/T\right)\right] \tag{6}$$

$$\tilde{D}_{\mu\nu} = \left(g_{\mu\nu} - \frac{p_\mu p_\nu}{m^2}\right) \tag{7}$$

where $n_B(x) = 1/(e^x - 1)$ denotes the Bose–Einstein distribution function. For the free TLM mode, we have

$$D^{\mathrm{TLM},0}_{ab,\mu\nu}(p) = -\delta_{ab}\left\{P^T_{\mu\nu}\left[\frac{i}{p^2} + 2\pi\delta\left(p^2\right) n_B\left(|p_0|/T\right)\right] - i\frac{u_\mu u_\nu}{\mathbf{p}^2}\right\}. \tag{8}$$

where

$$P^{00}_T = P^{0i}_T = P^{i0}_T = 0 \tag{9}$$

$$P^{ij}_T = \delta^{ij} - p^i p^j/\mathbf{p}^2\,. \tag{10}$$

TLM modes carry a color index 3 while TLH modes have a color indices 1 and 2. Notice the term $\propto u_\mu u_\nu$ in (8) describing the "propagation" of the A^3_0 field. Here $u_\mu = (1,0,0,0)$ represents the four velocities of the heat bath.

Resumming 1PI contributions to the polarization tensor, the scalar part of the tree-level propagators are modified in terms of screening functions $G_{\mathrm{TLH}}(p)$ and $G_{\mathrm{TLM}}(p)$ as[12]

$$\begin{aligned}
&\frac{i}{p^2-m^2} + 2\pi\delta(p^2-m^2)\,n_B(|p_0|/T) \\
&\quad\to \frac{i}{p^2 - (m^2 + \mathrm{Re}\,G_{\mathrm{TLH}}(p,T))} \\
&\qquad + 2\pi\rho_{\mathrm{TLH}}(p,T)\,n_B(|p_0|/T) \\
&\frac{i}{p^2} + 2\pi\delta(p^2)\,n_B(|p_0|/T) \\
&\quad\to \frac{i}{p^2 - \mathrm{Re}\,G_{\mathrm{TLM}}(p,T)} \\
&\qquad + 2\pi\rho_{\mathrm{TLM}}(p,T)\,n_B(|p_0|/T)\,,
\end{aligned} \tag{11}$$

[11] Pairs of TLH modes cannot be created or annihilated by quantum processes because these would need to invoke momentum transfers of at least twice their mass. This, however, is about 35 times larger than the maximally allowed resolving power in the effective theory. Due to the ground state possessing a positive energy density, it is possible that a preexisting TLH mode of positive energy correlates with the oppositely charged negative-energy state (a localized depression of the energy density of the ground state) for a time interval of length larger than $|\phi|^{-1}$; see calculations in [24–26]. Notice that this has nothing to do with the *creation* and subsequent *annihilation* of a pair of oppositely charged TLH modes.

[12] A discussion of the emergence of additional tensor structures $u_\mu u_\nu$ and $p_\mu u_\nu + p_\nu u_\mu$ due to loop effects is not important for our argument. To avoid a logical contradiction, the one-loop polarizations are first computed in real-time subject to the constraints (3) and (4). Subsequently, a continuation in the external momentum variable p^0 is performed to imaginary time. Then the resummation is carried out, and finally, the result is continued back to real time.

where the spectral functions at fixed spatial momentum $\mathbf{p}$ are defined as

$$\begin{aligned}
&\rho_{\mathrm{TLH}}(p^0, \mathbf{p}, T) \\
&\quad \equiv \frac{1}{\pi}\,\mathrm{Im}\,\frac{1}{p^2 - (m^2 + G_{\mathrm{TLH}}(p,T))} \\
&\quad = \frac{1}{\pi}\,\frac{\mathrm{Im}\,G_{\mathrm{TLH}}(p,T)}{\left(p^2 - m^2 - \mathrm{Re}\,G_{\mathrm{TLH}}(p,T)\right)^2 + \left(\mathrm{Im}\,G_{\mathrm{TLH}}(p,T)\right)^2} \\
&\rho_{\mathrm{TLM}}(p^0, \mathbf{p}, T) \\
&\quad \equiv \frac{1}{\pi}\,\mathrm{Im}\,\frac{1}{p^2 - G_{\mathrm{TLM}}(p,T)}, \\
&\quad = \frac{1}{\pi}\,\frac{\mathrm{Im}\,G_{\mathrm{TLM}}(p,T)}{\left(p^2 - \mathrm{Re}\,G_{\mathrm{TLM}}(p,T)\right)^2 + \left(\mathrm{Im}\,G_{\mathrm{TLM}}(p,T)\right)^2}\,.
\end{aligned} \tag{12}$$

From (12), it follows that powers of δ-functions of the same argument relax to powers of finite-widths (Lorentz-like) peaks of the same argument and thus to mathematically well-defined objects. The compositeness constraints and combinatorial factors are then modified compared with the tree-level ones. In practice, the computation of the pressure in a truncation at the two-loop level using tree-level propagators already yields results that are accurate on the 0.1% level [24–26].

4 Connected Bubble Diagrams

For the exact computation of thermodynamical quantities such as the pressure, all diagrams contributing to each mode's full propagator need to be known. Knowing the exact propagator (or the polarization tensor), in turn, fixes the exact dispersion law for each mode. This is important in applications [25, 26]. The polarization tensor is a sum over connected bubble diagrams (loop diagrams with no external legs) with one internal line of momentum p cut, such that the diagram remains connected and the two so-obtained external lines amputated. As a consequence, the vanishing of a connected bubble diagram due to a zero-measure support for its loop-momenta integrations implies that the associated contribution to a polarization tensor is also nil.

We conjecture that *all nonvanishing*, connected bubble diagrams enjoy the following property: For the total number V of their vertices, we have $V \leq V_{\max}$ with $V_{\max} < \infty$ provided that all 1PI contributions to the polarization tensor with up to $V_{\max}$ many vertices are resummed.

Let us now present our arguments in favor of this claim. The requirement that 1PI contributions to the polarization tensor are resummed assures that (1) all vertex constraints in (4) are operative (subject to slightly modified dispersion laws) and that (2) pinch singularities (powers of delta functions) do not occur because of the broadening of the spectral function of the respective mode's propagator, compared with Section 3. We consider the two cases where a connected bubble diagram *solely* contains (a) V_4 many four vertices and (b) V_3 many three vertices. This is relevant because the ratio of the number $\tilde{K}$ of independent radial loop-momentum variables (zero components and moduli of spatial momenta) to the number K of constraints on them is minimal for (a) and maximal for (b) at a given number $V = V_3 + V_4 \geq 2$ of vertices; see (16).

The relation between the number L of independent loop momenta, the number I of internal lines, and the number V of vertices for planar bubble diagrams is [27, 28]:

$$L = I - V + 1\,. \tag{13}$$

In the cases (a) and (b), we have in addition [27, 28]

$$I = 2\,V_4\,, \qquad \text{and} \qquad I = \frac{3}{2}\,V_3, \tag{14}$$

respectively. According to (3), we thus have in case (a) $2\,V_4$ constraints (propagators) and, according to (4), at least $\frac{3}{2}\,V_4$ constraints (vertices) on loop momenta. In case (a), this gives a total of $K \geq \frac{7}{2}\,V_4$ constraints. In case (b), we have a total of $K = \frac{3}{2}\,V_3$ constraints (only propagators). Combining (13) and (14), we obtain:

$$\begin{aligned}
&\text{for (a):}\ \ L = V_4 + 1 \quad \Rightarrow \quad \tilde{K} = 2\,V_4 + 2\,, \\
&\text{for (b):}\ \ L = \frac{V_3}{2} + 1 \quad \Rightarrow \quad \tilde{K} = V_3 + 2\,.
\end{aligned} \tag{15}$$

This yields:

$$\begin{aligned}
&\text{for (a):}\ \ \frac{\tilde{K}}{K} \leq \frac{4}{7}\left(1 + \frac{1}{V_4}\right), \\
&\text{for (b):}\ \ \frac{\tilde{K}}{K} = \frac{2}{3}\left(1 + \frac{2}{V_3}\right).
\end{aligned} \tag{16}$$

Obviously, the ratio $\tilde{K}/K$ is smaller in case (a) than it is in case (b). Notice that in case (a), the ratio $\frac{\tilde{K}}{K}$ is smaller than unity for $V_4 \geq 2$ while this happens for $V_3 \geq 6$ in case (b).

Now the constraints (3) and (4) are independent inequalities instead of independent equations and thus

do not identify independent hypersurfaces[13] in a $\tilde{K}$-dimensional Euclidean space $\mathbf{R}^{\tilde{K}}$. Rather, the inequalities (3) or (4) "fatten" hypersurfaces that would be obtained by setting their right-hand sides equal to zero.[14] As a consequence, the situation $\frac{\tilde{K}}{K} = 1$ fixes a discrete set of compact regions $C_{\tilde{K}}$ in $\mathbf{R}^{\tilde{K}}$ rather than a discrete set of points. If $\frac{\tilde{K}}{K}$ is sufficiently smaller than unity, which should be the case for sufficiently large V_4 and/or V_3 according to (16), then the associated diagram does not contribute: Fat hypersurfaces, specified by the number $\kappa \equiv K - \tilde{K}$ of constraints not used up for the determination of $C_{\tilde{K}}$, should have an intersection C_κ such that

$$C_\kappa \cap C_{\tilde{K}} = \emptyset \qquad (\kappa \gg 1). \tag{17}$$

Notice that according to (16)

$$\frac{3}{4}\,\tilde{K} \gtrsim \kappa \gtrsim \frac{1}{2}\,\tilde{K} \qquad \left(\tilde{K} \gg 1\right). \tag{18}$$

Although it is not rigorously guaranteed that $C_\kappa \cap C_{\tilde{K}} = \emptyset$ with κ ranging as in (18), this is, however, rather plausible.

For completeness, let us investigate the generalization of (13) to nonplanar bubble diagrams which can be considered spherical polyhedra with one face removed and a nonvanishing number of handles (genus $g > 0$). Equation (13) then generalizes as

$$V - I + L + 1 = 2 \quad \longrightarrow \quad V - I + L + 1 = 2 - 2g, \tag{19}$$

where again I is the number of internal lines, L the number of loops, and g represents the genus of the polyhedral surface (the number of handles). Notice that the right-hand side of the right-hand side equation is the full Euler-L' Huilliers characteristics. Reasoning as above but now based on the general situation of $g \geq 0$ expressed by the right-hand side equation in (19), we arrive at

$$\frac{\tilde{K}}{K} \leq \frac{4}{7}\left(1 + \frac{1}{V_4}\,(1 - 2g)\right) \quad (V = V_4)\,,$$

$$\frac{\tilde{K}}{K} \leq \frac{2}{3}\left(1 + \frac{2}{V_3}\,(1 - 2g)\right) \quad (V = V_3). \tag{20}$$

According to (20), the demand $\frac{\tilde{K}}{K} \leq 1$ for a compact support of the loop integrations is always satisfied for $g \geq 1$ since the number of vertices needs to be positive: $V_4 \geq 0$ and $V_3 \geq 0$. Recall that at $g = 0$, this is true only for $V_4 \geq 2$ and $V_3 \geq 6$, respectively. We thus conclude that bubble diagrams of a topology deviating from planarity are much more severely constrained than their planar counterparts.

5 Two Examples

Here we would like to demonstrate how severely conditions (3) and (4) constrain the loop momenta when increasing the number of vertices. Namely, we compare the situation of a two-loop diagram with that of a three-loop diagram.

Consider the diagrams in Fig. 2. Only TLH modes are involved which, due to constraint (5), propagate thermally, that is, on their mass shell. Diagram (a) is real while diagram (b) is purely imaginary, but here we are only interested in their moduli.

Diagram (a) We have $\tilde{K} = 4$ and $K = 3$. Thus, the region of integration for the radial loop variables cannot

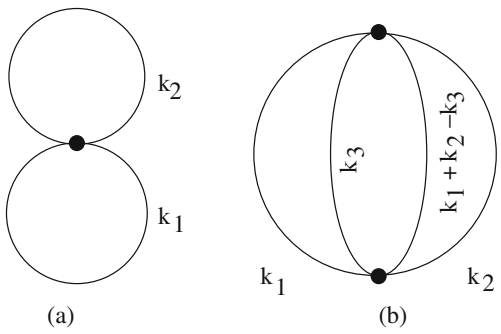

Fig. 2 **a** Two-loop and **b** three-loop diagram contributing to the pressure in the deconfining phase of SU(2) Yang–Mills thermodynamics. The *solid lines* are associated with thermal TLH-mode propagation

[13] By independent hypersurfaces H_i $(i = 1, \cdots, h \leq \tilde{K})$ in a $\tilde{K}$-dimensional Euclidean space $\mathbf{R}^{\tilde{K}}$, we mean that in a whole environment U of a point in their intersection $\bigcap_{i=1}^{h} H_i$, the normal vectors $\hat{n}_i$ to H_i (computed somewhere on $U \cap H_i$) are linearly independent. If $h = \tilde{K}$, then it follows that $\bigcap_{i=1}^{\tilde{K}} H_i$ is a discrete set of points.

[14] The case of a TLH mode, where only the thermal, on-shell part of the propagator contributes with a δ-function weight can be figured as the limit of a fat hypersurface subject to a regular weight acquiring zero width but now subject to a singular weight.

be compact. Let us show this explicitly. Before applying the constraints in (4), we have for diagram (a) [24]:

$$|\Delta P_a| = \frac{e^2\,\Lambda^4\,\lambda^{-2}}{(2\pi)^4} \times \sum_{\pm}\int dx_1\int dx_2\int dz_{12}\,\frac{x_1^2\,x_2^2}{\sqrt{x_1^2+4e^2}\sqrt{x_2^2+4e^2}} \times P_a^{\pm}(x_1,x_2,z_{12})\,n_B\left(2\pi\lambda^{-3/2}\sqrt{x_1^2+4e^2}\right) \times n_B\left(2\pi\lambda^{-3/2}\sqrt{x_2^2+4e^2}\right), \tag{21}$$

where $\lambda \equiv \frac{2\pi T}{\Lambda}$, $\mathbf{x}_i \equiv \frac{\mathbf{k}_i}{|\phi|}$, $x_i \equiv |\mathbf{x}_i|$ $(i=1,2)$, $z_{12} \equiv \cos\angle(\mathbf{x_1},\mathbf{x_2})$, and $P_a^{\pm}(x_1,x_2,z_{12})$ is given as:

$$P_a^{\pm}(x_1,x_2,z_{12}) \equiv \frac{1}{2}\left(6-\frac{x_1^2}{4e^2}-\frac{x_2^2}{4e^2}-\frac{x_1^2x_2^2}{16e^4}\left(1+z_{12}^2\right) \pm 2x_1x_2z_{12}\frac{\sqrt{x_1^2+4e^2}\sqrt{x_2^2+4e^2}}{16e^4}\right). \tag{22}$$

Applying the constraint $|(k_1+k_2)^2| \le |\phi|^2$, see (4), we have

$$\left|4e^2 \pm \sqrt{x_1^2+4e^2}\sqrt{x_2^2+4e^2} - x_1x_2z_{12}\right| \le \frac{1}{2}. \tag{23}$$

Only the minus sign is relevant ($e > \frac{1}{2\sqrt{2}}$) in (23). Thus, the expression within the absolute-value signs is strictly negative, and we have

$$z_{12} \le \frac{1}{x_1x_2}\left(4e^2-\sqrt{x_1^2+4e^2}\sqrt{x_2^2+4e^2}+\frac{1}{2}\right) \equiv g_{12}(x_1,x_2)\,. \tag{24}$$

Notice that $\lim_{x_1,x_2\to\infty} g_{12}(x_1,x_2) = -1$. Apart from a small compact region, where $g_{12}(x_1,x_2) \ge 1$ and which includes the point $x_1 = x_2 = 0$ in the $(x_1 \ge 0, x_2 \ge 0)$ quadrant, the admissible region of x_1, x_2 integration $(-1 \le g_{12}(x_1,x_2) < 1)$ is an infinite strip bounded by the two functions

$$x_2^u(x_1) = \frac{x_1+8e^2+\sqrt{1+16e^2}\sqrt{x_1^2+4e^2}}{8e^2}\,,$$
$$x_2^l(x_1) = \frac{x_1+8e^2-\sqrt{1+16e^2}\sqrt{x_1^2+4e^2}}{8e^2}. \tag{25}$$

We conclude that the integration region for radial loop momenta is not compact. Large x_1 and/or x_2 values are, however, Bose suppressed in (21), and the ratio $\frac{|\Delta P_a|}{P_{1-loop}}$, as a function of λ, is at most of order 10^{-5} [24].

Diagram (b) Here we have $\tilde{K} = 6$ and $K = 7$. According to the general arguments in Section 4, we know that the admissible region of radial loop integration either is compact or empty. After a rescaling of the loop momenta, conditions (4) are recast into

$$z_{12} \le \frac{1}{x_1x_2}\left(4e^2-\sqrt{x_1^2+4e^2}\sqrt{x_2^2+4e^2}+\frac{1}{2}\right) \equiv g_{12}(x_1,x_2)\,,$$
$$z_{13} \ge \frac{1}{x_1x_3}\left(-4e^2+\sqrt{x_1^2+4e^2}\sqrt{x_3^2+4e^2}-\frac{1}{2}\right) \equiv g_{13}(x_1,x_3)\,,$$
$$z_{23} \ge \frac{1}{x_2x_3}\left(-4e^2+\sqrt{x_2^2+4e^2}\sqrt{x_3^2+4e^2}-\frac{1}{2}\right) \equiv g_{23}(x_2,x_3), \tag{26}$$

where $z_{12} \equiv \cos\angle(\mathbf{x}_1,\mathbf{x}_2)$, $z_{13} \equiv \cos\angle(\mathbf{x}_1,\mathbf{x}_3)$, and $z_{23} \equiv \cos\angle(\mathbf{x}_2,\mathbf{x}_3)$. Notice that $\lim_{x_1,x_2\to\infty} g_{12} = -1 = -\lim_{x_1,x_3\to\infty} g_{13} = -\lim_{x_2,x_3\to\infty} g_{23}$. Before applying the constraints (26), diagram (b) reads

$$\begin{aligned}|\Delta P_b| \le{}& \frac{e^4\Lambda^4\lambda^{-2}}{2^3(2\pi)^6}\sum_{l,m,n=1}^{2}\int dx_1\int dx_2\int dx_3\int dz_{12}\int dz_{13}\int_{z_{23,l}}^{z_{23,u}} dz_{23} \\ &\times \frac{1}{\sqrt{(1-z_{12}^2)(1-z_{13}^2)-(z_{23}-z_{12}z_{13})^2}} \\ &\times \frac{x_1^2x_2^2x_3^2}{\sqrt{x_1^2+4e^2}\sqrt{x_2^2+4e^2}\sqrt{x_3^2+4e^2}} \\ &\times \delta\left(4e^2+(-1)^{l+m}\sqrt{x_1^2+4e^2}\sqrt{x_2^2+4e^2}-x_1x_2z_{12}\right. \\ &\quad -\left((-1)^{l+n}\sqrt{x_1^2+4e^2}\sqrt{x_3^2+4e^2}-x_1x_3z_{13}\right) \\ &\quad \left.-\left((-1)^{m+n}\sqrt{x_2^2+4e^2}\sqrt{x_3^2+4e^2}-x_2x_3z_{23}\right)\right) \\ &\times |P_b(\mathbf{x},\mathbf{z},l,m,n)|\,n_B\left(2\pi\lambda^{-3/2}\sqrt{x_1^2+4e^2}\right) \\ &\times n_B\left(2\pi\lambda^{-3/2}\sqrt{x_2^2+4e^2}\right)n_B\left(2\pi\lambda^{-3/2}\sqrt{x_3^2+4e^2}\right) \\ &\times n_B\left(2\pi\lambda^{-3/2}\left|(-1)^l\sqrt{x_1^2+4e^2}+(-1)^m\sqrt{x_2^2+4e^2}\right.\right. \\ &\quad \left.\left.+(-1)^n\sqrt{x_3^2+4e^2}\right|\right).\end{aligned} \tag{27}$$

where P_b is a function of $\mathbf{x} \equiv (x_1,x_2,x_3)$ and $\mathbf{z} \equiv (z_{12},z_{13},z_{23})$ emerging from Lorentz contractions and

thus is regular at $\mathbf{x} = 0$ (mass gap for TLH modes). In addition, we define:

$$z_{23,u} \equiv \cos\left|\arccos z_{12} - \arccos z_{13}\right| ,$$
$$z_{23,l} \equiv \cos\left|\arccos z_{12} + \arccos z_{13}\right| . \tag{28}$$

Let us now construct a useful compact embedding for the compact integration region in x_1, x_2, and x_3. First, consider the case that $x_1, x_2, x_3 \geq R > 0$. If $R > 1$, then conditions (26) and (28) do conflict.[15] The case that two out of the three variables x_1, x_2, and x_3 are larger than 2 while the third one is smaller than 1 is excluded by virtue of (26) since two angular integrations would then have no support. In a similar way, the case that one variable is larger than 2 while the other two are smaller than 1 is excluded by a vanishing support for two of the angular integrations. The situation that one variable is smaller than 1, another variable is in between 1 and 2, and the third variable is larger than 2 is excluded because one angular integration would then have no support. On the other hand, the situation that two variables are smaller than 1 while the third one is in between 1 and 2 is not excluded. This goes also for the case that two variables are in between 1 and 2 while the third one is smaller than 1. We conclude that the region of integration allowed by the conditions (26) and by (28) is compact and bounded by a sphere of radius 3 which is centered at $\mathbf{x} = 0$. Hence, there is a qualitative difference with diagram (a) where the region of x_1-x_2 integration is noncompact.

Solving $g(\mathbf{x}, \mathbf{z}) = 0$ for x_1, where g is the function defined by the argument of the delta function in (27), we have

$$x_1 = \frac{ac}{b^2 - c^2} + (-1)^n \sqrt{\left(\frac{ac}{b^2 - c^2}\right)^2 - \frac{4e^2b^2 - a^2}{b^2 - c^2}}, \tag{29}$$

where

$$c \equiv x_2 z_{12} - x_3 z_{13} ,$$
$$a \equiv (-1)^{m+n} \sqrt{x_2^2 + 4e^2}\sqrt{x_3^2 + 4e^2} - x_2 x_3 z_{23} - 4e^2 ,$$
$$b \equiv (-1)^l \sqrt{x_2^2 + 4e^2} + (-1)^{m+1} \sqrt{x_3^2 + 4e^2}. \tag{30}$$

We present numerical results for the temperature dependence of the estimate for the modulus of diagram (b) elsewhere [29].

[15] The truth of this and the following statements is easily checked numerically.

6 Conclusions

We have discussed how constraints on loop momenta, which emerge in the effective theory for the deconfining phase of SU(2) Yang–Mills thermodynamics [4, 5], enforce a loop expansion with properties dissenting from those known in perturbation theory. Namely, we have argued that, modulo 1PI resummations, there is only a finite number of connected bubble diagrams contributing to the expansion of thermodynamical quantities or, by cutting one internal line, to the expansion of the polarization tensor. Our arguments of Section 4 apply equally well to the SU(3) case. Because the quasiparticle mass spectrum is slightly more involved, there are mild modifications of Sections 2, 3, and 5 when going from SU(2) to SU(3); see [4, 5].

The reason for the improved convergence properties of loop expansions in the effective theory is clear: The spatial coarse graining over both topological and plane-wave fluctuations self-consistently generates both a natural resolving power as a function of T and Λ and quasiparticle masses on tree level. As a consequence, residual quantum fluctuations have a small action as compared to $\hbar$.

Acknowledgements The author would like to acknowledge useful and stimulating conversations with Francesco Giacosa, Dariush Kaviani, Jan Pawlowski, and Markus Schwarz.

References

1. A.D. Linde, Phys. Lett. B **96**, 289 (1980)
2. A.M. Polyakov, Phys. Lett. B **59**, 82 (1975)
3. F. Giacosa, R. Hofmann, M. Schwarz, **A21**, 2709–2715, hep-ph/0604174 (2006)
4. R. Hofmann, Int. J. Mod. Phys. A **20**, 4123 (2005)
5. R. Hofmann, Mod. Phys. Lett. A **21**, 999 (2006)
6. U. Herbst, R. Hofmann, hep-th/0411214 (2004)
7. B.J. Harrington, H.K. Shepard, Phys. Rev. D **17**, 105007 (1978)
8. R. Fariello, H. Forkel, G. Krein, Phys. Rev. D **72**, 105015 (2005)
9. G.'t Hooft, Nucl. Phys. B **33**, 173 (1971)
10. G.'t Hooft, M.J.G. Veltman, Nucl. Phys. B **44**, 189 (1972)
11. G.'t Hooft, Int. J. Mod. Phys. A **20**, 1336 (2005) [arXiv:hep-th/0405032]
12. W. Nahm, Phys. Lett. B **90**, 413 (1980)
13. W. Nahm, *Lect. Notes in Physics.*, vol. 201, eds. by G. Denaro, et al., p. 189 (1984)
14. K.-M. Lee, C.-H. Lu, Phys. Rev. D **58**, 025011 (1998)
15. T.C. Kraan, P. van Baal, Nucl. Phys. B **533**, 627 (1998)
16. T.C. Kraan, P. van Baal, Phys. Lett. B **428**, 268 (1998)
17. T.C. Kraan, P. van Baal, Phys. Lett. B **435**, 389 (1998)
18. D. Diakonov, N. Gromov, V. Petrov, S. Slizovskiy, Phys. Rev. D **70**, 036003, hep-th/0404042 (2004)
19. D.J. Gross, R.D. Pisarski, L.G. Yaffe, Rev. Mod. Phys. **53**, 43 (1981)

20. P. Giovannangeli, C.P. Korthals Altes, Talk given at 19th International Symposium on Lattice Field Theory (Lattice 2001), Berlin, Germany, 19–24 Aug 2001, Nucl. Phys. Proc. Suppl. **106**, 616 (2002)
21. A.M. Polyakov, Phys. Lett. B **59**, 82 (1975)
22. A.M. Polyakov, Phys. Lett. B **72**, 477 (1978)
23. P. Gerold, E.-M. Ilgenfritz, M. Müller-Preussker, Nucl. Phys. **B760**, 1–37, hep-ph/0607315 (2007)
24. U. Herbst, R. Hofmann, J. Rohrer, Acta Phys. Pol. B **36**, 881 (2005)
25. M. Schwarz, R. Hofmann, F. Giacosa, Int. J. Mod. Phys., **A22**, 1213–1238, hep-th/0603078 (2007)
26. M. Schwarz, R. Hofmann, and F. Giacosa, JHEP **0702**, 091, hep-ph/0603174 (2007)
27. S. Weinberg, *The quantum theory of fields*, vol. I (Cambridge University Press, Cambridge, 1995), pp. 282–286
28. J. Zinn-Justin, *Quantum field theory and critical phenomena* (Clarendon, Oxford, 1989), p. 126
29. D. Kaviani and R. Hofmann, Mod. Phys. Lett A, **22**, 2343 (2007), arXiv:0704.3326 [th]